Journal of *Marine Science and Engineering*

MDPI

Article

Abnormal Data Elimination-Based Underwater 3D Magnetic Induction Localization Method

Meiyan Zhang [1], Ning Zhang [2], Niaz Ahmed [3], Zhou Yu [4] and Wenyu Cai [2,*]

[1] College of Electrical Engineering, Zhejiang University of Water Resources and Electric Power, Hangzhou 310018, China
[2] School of Electronics Information, Hangzhou Dianzi University; Hangzhou 310018, China
[3] School of Engineering, FAST National University of Computer and Emerging Sciences (FAST-NUCES), Islamabad 44000, Pakistan
[4] Hangzhou Aohai Ocean Engineering Technology Co., Ltd., Hangzhou 310018, China
* Correspondence: dreampp2000@163.com

Abstract

To address the problem of three-dimensional (3D) localization in underwater environments, this paper proposes a 3D positioning method based on magnetic induction communication (MI in short). Dual transmitters equipped with 3D coils are used to transmit magnetic field signals, while a single receiver with 3D coils is adopted to receive signals. Three-dimensional position calculation is realized by collecting induced voltage from the receiving 3D coils, which enables any device at a known position in space to provide positioning services for other devices. To eliminate abnormal data and suppress environmental noise interference in underwater received signals and further improve positioning performance, an improved density clustering algorithm named the Density-Based Spatial Clustering Method in Magnetic Positioning is proposed to remove erroneous positioning data. In addition, Kalman filtering is introduced to jointly suppress environmental noise interference. Experimental results demonstrate that the average positioning error of the proposed localization method is 0.67 m and maximum positioning error is 0.83 m; therefore, this paper provides a novel technical solution for underwater positioning in non-line-of-sight environments.

Keywords: magnetic induction localization; magnetic induction communication; clustering algorithm; underwater positioning technology

1. Introduction

Underwater three-dimensional positioning provides essential support for underwater engineering, but it still faces challenges such as strong noise, signal attenuation, and large positioning errors in complex marine environments [1]. Traditional radio frequency communication technologies are limited in occluded environments such as underwater, underground, indoor, and in vivo scenarios. In contrast, low-frequency magnetic induction communication has become a research hotspot for localization in such scenarios due to its non-line-of-sight penetration capability and anti-interference characteristics [2]. In this paper, we apply magnetic induction communication and localization into underwater scenarios.

There are some related works on magnetic induction positioning technology. Pan et al. used a sensor array to localize a magnetic capsule, which was intended for in vivo positioning [3]. Abrudan et al. investigated the effects of rocks and minerals on underground magnetic induction communication and localization [4], and achieved sub-meter-level positioning using 3D coils through iterative optimization among multiple

Check for updates

Academic Editor: Weicheng Cui

Received: 20 May 2026
Revised: 26 June 2026
Accepted: 3 July 2026
Published: 4 July 2026

Copyright: © 2026 by the authors. Licensee MDPI, Basel, Switzerland. This article is an open access article distributed under the terms and conditions of the Creative Commons Attribution (CC BY) license.

nodes [5], where accuracy was improved via iteration. Chavda et al. realized underground localization in a 1 m × 1 m × 0.45 m sand pit and enhanced accuracy by increasing the number of transmitters [6]. Wang et al [7] performed underwater localization using 3D coils in a 2 m water tank under relatively ideal conditions. Pasku et al. achieved indoor localization with an error of approximately 0.9 m using low-frequency magnetic fields [8], and later integrated pedestrian inertial navigation with magnetic positioning in a loosely coupled manner to realize mobile localization with 1–2 m error [9]. The former work mainly verified the localization theory, while the latter improved accuracy by fusing magnetic positioning and inertial navigation data, but neither addressed measurement errors. Hehn et al. [10] achieved sub-meter indoor localization with 3D coils and analyzed angular deviations, yet also lacked error processing. In practice, strong magnetic interference, coil alignment errors during testing [11], and underwater path loss [12] all introduce disturbances and cause measurement errors. Erroneous data often appear during data acquisition in real applications. This paper analyzes measured data and extracts two major interference patterns, which are eliminated by targeted algorithms. Inspired by electromagnetic induction law, a 3D localization method based on magnetic induction communication is proposed, in which dual transmitters (3D coils) send magnetic field signals and a single receiver (3D coils) receives signals. Localization is realized by sampling voltages on the 3D receiving coils during magnetic induction communication, helping any device at a known spatial position to provide positioning services for other devices.

In practice, strong magnetic interference, coil alignment errors, and underwater path loss cause measurement errors. This paper analyzes the induced voltage as measured dataand extracts two major interference types: (1) a small number of outliers with large positioning errors caused by measurement faults; (2) a large number of noisy data points with moderate errors caused by environmental noise, sensor precision, and coil misalignment. To address these issues, this paper proposes DBSCAN-MP clustering to eliminate outliers and Kalman filtering to suppress noise. Extensive simulations and experiments are provided to verify the proposed method. Finally, experimental results show an average error of 0.67 m and maximum error of 0.83 m. To the best of our knowledge, this is the first time the Density-Based Spatial Clustering Method has been applied in magnetic positioning.

The remainder of this paper is organized as follows. Section 2 provides an underwater 3D localization model, Section 3 proposes the Density-Based Spatial Clustering Method in Magnetic Positioning in detail, simulation and experimental results are proposed in Section 4. Section 5 is the conclusion.

2. Underwater 3D Localization Model

In this paper, we establish an underwater 3D positioning model. Underwater magnetic induction communication-related works have been discussed in Refs. [13–15]. A typical three-dimensional localization scenario is shown in Figure 1.

According to the classic Biot–Savart law, the magnetic moment generated by a current-carrying coil is expressed as:

$$\vec{\boldsymbol{M}} = N_t I_t S_t \vec{\boldsymbol{m}} \tag{1}$$

where the direction of the magnetic moment $\vec{\boldsymbol{m}}$ is the normal vector of the coil, S_t is the area of the transmitting coil, N_t is the number of turns, and I_t is the driving current.

In the near magnetic field region, the magnetic flux density $\vec{\mathbf{B}}$ at an arbitrary position $\mathrm{P}[x, y, z]$ can be expressed as

$$\vec{\mathbf{B}} = \frac{\mu}{4\pi d^2 \sqrt{\left(r_t^2 + d^2\right)^3}} \cdot \left[3\left(\vec{\mathbf{M}} \cdot \vec{\mathbf{d}}\right)\vec{\mathbf{d}} - \vec{\mathbf{M}} d^2\right] \tag{2}$$

where $\vec{\mathbf{d}} = x\vec{\mathbf{x}} + y\vec{\mathbf{y}} + z\vec{\mathbf{z}}$ is the direction vector from the current-carrying coil to point P, and $d = \left\|\vec{\mathbf{d}}\right\| = |x\vec{\mathbf{x}} + y\vec{\mathbf{y}} + z\vec{\mathbf{z}}|$ is the distance from the current-carrying coil to point P. Here, r is the radius of the transmitting coil, and μ is the magnetic permeability of the medium.

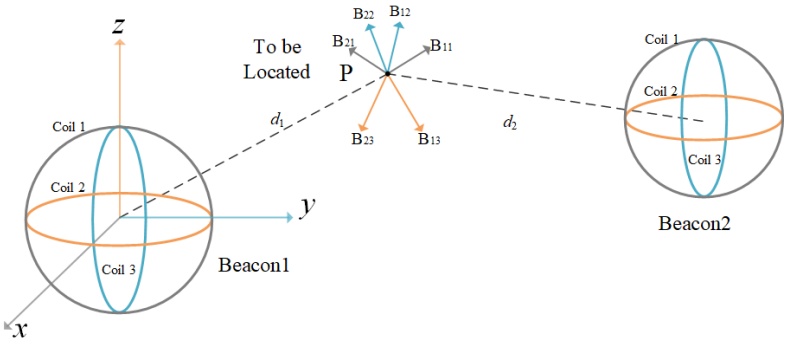


Figure 1. 3D localization scenario based on magnetic induction communication.

When the normal vector of the current-carrying coil is aligned with the x-axis, i.e.,

$$\vec{\mathbf{M}} = S_t N_t I_t \vec{\mathbf{x}}, \tag{3}$$

substituting $\vec{\mathbf{d}} = x\vec{\mathbf{x}} + y\vec{\mathbf{y}} + z\vec{\mathbf{z}}$ and Equation (3) into Equation (2), the magnetic flux density along the x-axis can be obtained as

$$\vec{\mathbf{B}}_x = \frac{\mu S_t N_t I_t}{4\pi d^2 \sqrt{\left(r_t^2 + d^2\right)^3}} \cdot \left[\left(2x^2 - y^2 - z^2\right)\vec{\mathbf{x}} + (3xy)\vec{\mathbf{y}} + (3xz)\vec{\mathbf{z}}\right] \tag{4}$$

Similarly, when the normal vector of the current-carrying coil is aligned with the y-axis and z-axis, the magnetic flux density at an arbitrary position in space is given by

$$\vec{\mathbf{B}}_y = \frac{\mu S_t N_t I_t}{4\pi d^2 \sqrt{\left(r_t^2 + d^2\right)^3}} \cdot \left[(3xy)\vec{\mathbf{x}} + (2y^2 - x^2 - z^2)\vec{\mathbf{y}} + (3yz)\vec{\mathbf{z}}\right] \tag{5}$$

$$\vec{\mathbf{B}}_z = \frac{\mu S_t N_t I_t}{4\pi d^2 \sqrt{\left(r_t^2 + d^2\right)^3}} \cdot \left[(3xz)\vec{\mathbf{x}} + (3yz)\vec{\mathbf{y}} + (2z^2 - x^2 - y^2)\vec{\mathbf{z}}\right] \tag{6}$$

Combining Equations (4)–(6) into a matrix form yields

$$\begin{bmatrix} \vec{\mathbf{B}}_x \\ \vec{\mathbf{B}}_y \\ \vec{\mathbf{B}}_z \end{bmatrix} = \frac{\mu S_t N_t I_t}{4\pi d^2 \sqrt{\left(r_t^2 + d^2\right)^3}} \mathbf{T} \begin{bmatrix} \vec{\mathbf{x}} \\ \vec{\mathbf{y}} \\ \vec{\mathbf{z}} \end{bmatrix} \tag{7}$$

where

$$\vec{\mathbf{T}} = \begin{bmatrix} \vec{\mathbf{t_1}} \\ \vec{\mathbf{t_2}} \\ \vec{\mathbf{t_3}} \end{bmatrix} = \begin{bmatrix} 2x^2 - y^2 - z^2 & 3xy & 3xz \\ 3xy & 2y^2 - x^2 - z^2 & 3yz \\ 3xz & 3yz & 2z^2 - x^2 - y^2 \end{bmatrix} \tag{8}$$

The actual triaxial coil magnetic induction model is shown in Figure 2. The beacon node generates a magnetic field distribution, and the receiver estimates the position based on this distribution. Assume that in the triaxial coil of the beacon node, the normal vector of the T_1 axis is aligned with the x-axis, the normal vector of the T_2 axis is aligned with the y-axis, and the normal vector of the T_3 axis is aligned with the z-axis. The triaxial magnetic induction intensity at the center of the receiving coil is

$$\begin{cases} \vec{\mathbf{B}}_1 = \dfrac{\mu S_t N_t I_{t1}}{4\pi d^2 \sqrt{\left(r_t^2 + d^2\right)^3}} \cdot \vec{\mathbf{t}}_1 = \dfrac{\mu S_t N_t I_{t1}}{4\pi d^2 \sqrt{\left(r_t^2 + d^2\right)^3}} \cdot \begin{bmatrix} 2x^2 - y^2 - z^2 \\ 3xy \\ 3xz \end{bmatrix} \\ \vec{\mathbf{B}}_2 = \dfrac{\mu S_t N_t I_{t2}}{4\pi d^2 \sqrt{\left(r_t^2 + d^2\right)^3}} \cdot \vec{\mathbf{t}}_2 = \dfrac{\mu S_t N_t I_{t2}}{4\pi d^2 \sqrt{\left(r_t^2 + d^2\right)^3}} \cdot \begin{bmatrix} 3xy \\ 2y^2 - x^2 - z^2 \\ 3yz \end{bmatrix} \\ \vec{\mathbf{B}}_3 = \dfrac{\mu S_t N_t I_{t3}}{4\pi d^2 \sqrt{\left(r_t^2 + d^2\right)^3}} \cdot \vec{\mathbf{t}}_3 = \dfrac{\mu S_t N_t I_{t3}}{4\pi d^2 \sqrt{\left(r_t^2 + d^2\right)^3}} \cdot \begin{bmatrix} 3xz \\ 3yz \\ 2z^2 - x^2 - y^2 \end{bmatrix} \end{cases} \tag{9}$$

where $B_i, i \in \{1,2,3\}$ is the magnetic induction intensity generated by coil T_i; S_t is the area of the transmitting coil; N_t is the number of turns of the transmitting coil; r_t is the radius of the transmitting coil; and I_{t1}, I_{t2}, and I_{t3} represent the currents of T_1, T_2, and T_3, respectively.

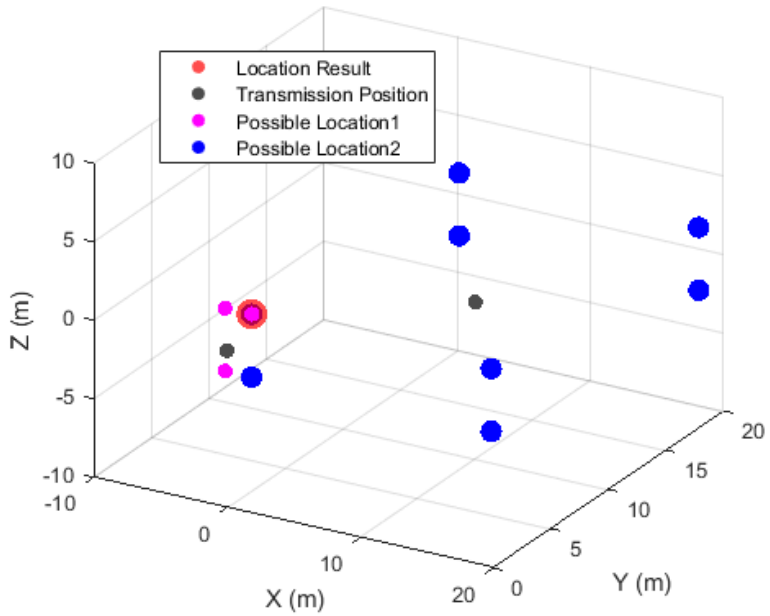


Figure 2. Possible results with theoretical voltage value.

The normal vector matrix of three receiving coils is defined as a square matrix:

$$\mathbf{V} = \begin{bmatrix} \vec{\mathbf{n}}_1 \\ \vec{\mathbf{n}}_2 \\ \vec{\mathbf{n}}_3 \end{bmatrix} = \begin{bmatrix} x_1 & y_1 & z_1 \\ x_2 & y_2 & z_2 \\ x_3 & y_3 & z_3 \end{bmatrix} \tag{10}$$

The magnetic flux generated by the transmitting coil $T_i, i \in \{1,2,3\}$ and passing through the receiving coil $R_j, j \in \{1,2,3\}$ is

$$\Phi_{ij} = B_i \cdot S_j = \frac{\mu N_t I_t S_t S_r}{4\pi d^2 \sqrt{\left(r_t^2 + d^2\right)^3}} t_i n_j \tag{11}$$

Using the mutual inductance formula $H_{ij} = N_r \Phi_{ij} / I_{ti}$, the mutual inductance between the transmitting coil and the receiving coil can be calculated as

$$\mathbf{H} = \begin{bmatrix} H_{11} & H_{12} & H_{13} \\ H_{21} & H_{22} & H_{23} \\ H_{31} & H_{32} & H_{33} \end{bmatrix} = \frac{\mu N_t N_r S_t S_r}{4\pi d^2 \sqrt{\left(r_t^2 + d^2\right)^3}} \cdot \mathbf{T} \cdot \mathbf{V}^{\mathrm{T}} \tag{12}$$

Let the transmitting coils T_1, T_2 and T_3 generate sinusoidal signals. The nine-channel induced voltage intensity matrix (three coils to transmit and three coils to receive) obtained at three receiving coils is

$$\mathbf{U}_R = \begin{bmatrix} U_{R1} \\ U_{R2} \\ U_{R3} \end{bmatrix} = \begin{bmatrix} U_{11} & U_{12} & U_{13} \\ U_{21} & U_{22} & U_{23} \\ U_{31} & U_{32} & U_{33} \end{bmatrix} \tag{13}$$

where U_{ij} denotes the voltage amplitude generated by the induced signal from transmitting coil T_i on receiving coil R_j, $i, j \in \{1, 2, 3\}$.

According to the formula $U_{ij} = j\omega H_{ij} I_{ti}$, the receiver induced voltage can be calculated from the mutual inductance, which yields

$$\begin{cases} \|U_{R1}\|^2 = \omega^2 I_{t1}^2 \left(\frac{\mu \pi^2 N_t N_r r_t^2 r_r^2}{4\pi d^2 \sqrt{\left(r_t^2 + d^2\right)^3}} \right)^2 \|t_1\|^2 \\ \|U_{R2}\|^2 = \omega^2 I_{t2}^2 \left(\frac{\mu \pi^2 N_t N_r r_t^2 r_r^2}{4\pi d^2 \sqrt{\left(r_t^2 + d^2\right)^3}} \right)^2 \|t_2\|^2 \\ \|U_{R3}\|^2 = \omega^2 I_{t3}^2 \left(\frac{\mu \pi^2 N_t N_r r_t^2 r_r^2}{4\pi d^2 \sqrt{\left(r_t^2 + d^2\right)^3}} \right)^2 \|t_3\|^2 \end{cases} \tag{14}$$

In far-field magnetic induction positioning scenarios, the positioning distance is generally much larger than the transceiver coil's radius, so the coils can be regarded as magnetic dipoles. Hence, Equation (13) above can be simplified to

$$\begin{cases} \|U_{R1}\|^2 = \omega^2 I_{t1}^2 \left(\frac{\mu \pi^2 N_t N_r r_t^2 r_r^2}{4\pi d^5} \right)^2 \|t_1\|^2 \\ \|U_{R2}\|^2 = \omega^2 I_{t2}^2 \left(\frac{\mu \pi^2 N_t N_r r_t^2 r_r^2}{4\pi d^5} \right)^2 \|t_2\|^2 \\ \|U_{R3}\|^2 = \omega^2 I_{t3}^2 \left(\frac{\mu \pi^2 N_t N_r r_t^2 r_r^2}{4\pi d^5} \right)^2 \|t_3\|^2 \end{cases} \tag{15}$$

$$d = \left(\frac{3\omega^2 \pi^2 \left(\mu N_t N_r r_t^2 r_r^2\right)^2}{8\left(\|\mathbf{U}_{R1}\|^2 / I_{t1}^2 + \|\mathbf{U}_{R2}\|^2 / I_{t2}^2 + \|\mathbf{U}_{R3}\|^2 / I_{t3}^2 \right)} \right)^{\frac{1}{6}} \tag{16}$$

After calculating d, substitute Equation (15) into Equation (14) to obtain the coordinates of the receiver, i.e.,

$$\begin{cases} x = \pm \sqrt{\max\left(\frac{\|\mathbf{U}_{R1}\|^2}{3d^2 h^2 \omega^2 I_{t1}^2} - \frac{d^2}{3}, 0 \right)} \\ y = \pm \sqrt{\max\left(\frac{\|\mathbf{U}_{R2}\|^2}{3d^2 h^2 \omega^2 I_{t2}^2} - \frac{d^2}{3}, 0 \right)} \\ z = \pm \sqrt{\max\left(\frac{\|\mathbf{U}_{R3}\|^2}{3d^2 h^2 \omega^2 I_{t3}^2} - \frac{d^2}{3}, 0 \right)} \end{cases} \tag{17}$$

where $h = \mu N_t N_r S_t S_r / (4\pi d^5)$ is the intermediate coefficient of the mutual inductance **H**. The estimated coordinates have eight possible solutions $P_{1i} = [x, y, z], i \in \{1, 2, \ldots, 8\}$, which are symmetrically distributed in the eight octants of the Cartesian coordinate system.

Similarly, by placing a second triaxial transmitting coil as a beacon at position $[X_{B2}, Y_{B2}, Z_{B2}]$, another set of eight possible coordinates $P_{2i} = [x, y, z], i \in \{1, 2, \ldots, 8\}$ can be calculated at the receiving coil.

Perform coordinate transformation on the coordinates of P_{2i}, i.e., the actual coordinates are $P_{2i} = [x + X_{B2}, y + Y_{B2}, z + Z_{B2}], i \in \{1, 2, \ldots, 8\}$.

The nearest positioning points between two sets of coordinates are obtained via Equation (17):

$$\min\left(\left\|P_{1i}, P_{2j}\right\|\right), \forall i, j \in \{1, 2, \ldots, 8\} \tag{18}$$

where $\left\|P_{1i}, P_{2j}\right\|$ denotes the Euclidean distance between the two points. Two coordinate values with the smallest Euclidean distance are recorded, and the midpoint of these two coordinates is taken as the positioning result $P = [x, y, z]$.

3. DBSCAN-MP Algorithm for Abnormal Data Processing

In actual voltage acquisition, considerable interference and abnormal data exist. Therefore, based on the density clustering method DBSCAN (Density-Based Spatial Clustering of Applications with Noise), this paper proposes an improved density clustering algorithm suitable for magnetic positioning: DBSCAN-MP (Density-Based Spatial Clustering Methods in Magnetic Positioning).

DBSCAN partitions data by neighborhood radius ε and minimum core point number *MinPts*. For any data point in the dataset, the set of neighboring points within its neighborhood radius is defined as

$$N_\varepsilon(p) = \{q \in D \mid \mathrm{dist}(p, q) \leq \varepsilon\} \tag{19}$$

where p and q are 3×3 voltage matrices obtained from theoretical calculations, and $\mathrm{dist}(\cdot)$ is the distance metric.

The 'dist()' function in DBSCAN typically computes the Euclidean distance:

$$\mathrm{dist}(p, q) = \left\| \begin{bmatrix} U_{11} & U_{12} & U_{13} \\ U_{21} & U_{22} & U_{23} \\ U_{31} & U_{32} & U_{33} \end{bmatrix}_p - \begin{bmatrix} U_{11} & U_{12} & U_{13} \\ U_{21} & U_{22} & U_{23} \\ U_{31} & U_{32} & U_{33} \end{bmatrix}_q \right\|^2 \tag{20}$$

where the symbol $\| \cdot \|^2$ denotes the sum of the squares of all elements in the matrix.

From Equation (15), it can be observed that when the transmitting currents of each coil are the same, the distance from the positioning point to the origin is inversely proportional to $\|\mathbf{U}_{R1}\|^2 + \|\mathbf{U}_{R2}\|^2 + \|\mathbf{U}_{R3}\|^2$. From Equation (16), it can be seen that the positioning coordinates $[x, y, z]$ are correlated with the ratios of $\|\mathbf{U}_{R1}\|^2$, $\|\mathbf{U}_{R2}\|^2$ and $\|\mathbf{U}_{R3}\|^2$. Therefore, the DBSCAN-MP method proposed in this paper performs clustering by calculating the overall distance feature and the position distribution feature using 'cha1()' and 'cha2()', respectively:

$$\begin{cases} C_1 = \mathrm{cha1}(p) = \|\mathbf{U}_{R1}\|^2 + \|\mathbf{U}_{R2}\|^2 + \|\mathbf{U}_{R3}\|^2 \\ C_2 = \mathrm{cha2}(p) = \left(\frac{\|\mathbf{U}_{R1}\|^2}{\|\mathbf{U}_{R2}\|^2} + \frac{\|\mathbf{U}_{R1}\|^2}{\|\mathbf{U}_{R3}\|^2} + \frac{\|\mathbf{U}_{R2}\|^2}{\|\mathbf{U}_{R3}\|^2} \right) \end{cases} \tag{21}$$

where C_1 is the overall distance feature of data point p, and C_2 is the position distribution feature of data point p.

The DBSCAN-MP method uses the $\text{dist}_{\text{cha}}(p,q)$ function to find the set of neighboring points $N_\epsilon(p)$ within the neighborhood radius $\epsilon = \{\epsilon_1, \epsilon_2\}$ for any data point p:

$$\begin{cases} N_\epsilon(p) = \{q \in D \mid \text{dist}_{\text{cha1}}(p,q) \le \epsilon_1, \text{dist}_{\text{cha2}}(p,q) \le \epsilon_2\} \\ \text{dist}_{\text{cha1}}(p,q) = \lambda_1(C_{1p} - C_{1q}) \\ \text{dist}_{\text{cha2}}(p,q) = \lambda_2(C_{2p} - C_{2q}) \end{cases} \tag{22}$$

where ϵ_1, ϵ_2 are the radii corresponding to features C_1 and C_2, respectively; λ_1 and λ_2 are feature weights. The weight λ_1 is related to the C_1 features of all data points, and λ_2 is a step weight, whose specific calculation formulas are shown in Equations (23) and (24):

$$\lambda_1 = \lambda_{1\max} \times \frac{1}{N} \times \sum_{x \in D} C_{1_x} \tag{23}$$

$$\lambda_2 = \begin{cases} 0, & \text{if } U_1 = 0 \parallel U_2 = 0 \parallel U_3 = 0 \\ \lambda_{2\max}, & \text{otherwise} \end{cases} \tag{24}$$

where $\lambda_{1\max}$ and $\lambda_{2\max}$ are user-defined weights, and N is the size of dataset D.

Meanwhile, the minimum number of points 'minPts' is used to control the minimum number of data points contained in a cluster. Let $|N_\epsilon(p)|$ denote the number of data points in the neighborhood set $N_\epsilon(p)$. When $|N_\epsilon(p)| \ge$ minPts, $N_\epsilon(p)$ is considered a valid cluster.

The procedure of DBSCAN-MP is given in Algorithm 1.

Algorithm 1 The proposed DBSCAN-MP Algorithm

Require: Voltage dataset $D = \{d_1, d_2, \ldots, d_N\}$, radius ε, $MinPts$
Ensure: Clean voltage dataset U

```
C ← 0
for all p ∈ D do
  if p is visited then
    continue
  end if
  Mark p as visited
  Obtain neighborhood set N_ε(p)
  if |N_ε(p)| < MinPts then
    Mark p as noise
  else
    C ← C + 1
    Create new cluster C and add p to it
    for all q ∈ N_ε(p) do
      if q is not visited then
        Mark q as visited
        Obtain N_ε(q)
        if |N_ε(q)| ≥ MinPts then
          Merge N_ε(q) into N_ε(p)
        end if
      end if
      if q is not assigned to any cluster then
        Add q to cluster C
      end if
    end for
  end if
end for
Collect valid points from all clusters as dataset U
```

To suppress interference caused by sensor precision and coil alignment errors, Kalman filtering is adopted. The process noise covariance $Q = 0.001$ and measurement noise covariance $R = 0.2$ are set, so that the filter trusts the state prediction model and suppresses high-volume weak noise. The above parameters are set following existing Kalman filtering methods.

4. Simulation and Experimental Results

4.1. Simulation Setup and Results

These important algorithm parameters in the proposed algorithm used in the simulation and experiment are listed in Table 1. The radius and turns of coils are decided by our magnetic induction communication system, and the two weights are decided by empirical equations. Five localization methods are compared: raw positioning, Kalman filtering, conventional DBSCAN, DBSCAN-MP, and DBSCAN-MP combined with Kalman filtering.

Table 1. Simulation parameters.

Parameter	Value
Radius of transmitting coil	0.1 m
Radius of receiving coil	0.1 m
Turns of transmitting coil	50
Turns of receiving coil	50
Permeability of vacuum	$4\pi \times 10^{-7}$ H/m
Magnetic field frequency	$2\pi \times 125{,}000$ rad/s
Excitation current of transmitter	0.25 A
Weight for distance feature λ_1	0.01
Weight for position feature λ_2	0.33
Density threshold minPts	15

Two beacons are placed at $[0, 0, 0]$ and $[10, 10, 0]$, and the receiver is at $[2, 4, 2]$. Using ideal voltage data, the positioning result is $[2.0001, 4.0011, 2.0010]$, with millimeter-level error caused by the magnetic dipole approximation.

Under 10 dB SNR, the positioning result becomes $[1.6030, 4.4054, 1.0842]$. Under 5 dB SNR, severe outliers appear, e.g., $[5.3306, -1.8880, 1.4266]$.

The simulation scenario is shown in Figure 2. The coordinates of the transmitting beacons are $[0, 0, 0]$ and $[10, 10, 0]$, and the position of the receiver is $[2, 4, 2]$. Positioning is performed using the theoretical voltage, and two groups of 16 possible positions are obtained. The coordinate point obtained by Equation (17) is $[2.0001, 4.0011, 2.0010]$. The difference from the actual position $[2, 4, 2]$ is because the coil is regarded as a magnetic dipole in Equation (14), and the positioning error obtained by Equation (14) is at the millimeter level.

After adding Gaussian noise, positioning is carried out at a signal-to-noise ratio of 10 dB, and errors appear in the positioning results. The positioning result in Figure 3 is $[1.6030, 4.4054, 1.0842]$, showing a sub-meter-level positioning error due to noise.

As the noise increases gradually, the positioning error becomes larger at a signal-to-noise ratio of 5 dB. Even completely wrong positioning results may occur, as shown in Figure 4, where the positioning result is $[5.3306, -1.8880, 1.4266]$. This is because the Gaussian noise may be extremely large at a certain moment, leading to a significant error in the positioning result of Equation (16).

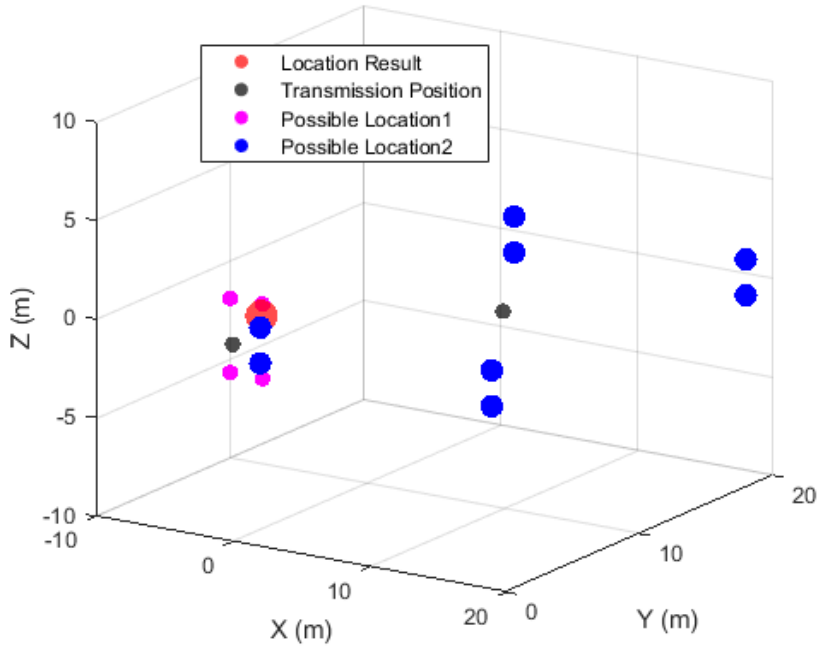


Figure 3. Possible results with theoretical voltage mixed with 10 dB SNR noise.

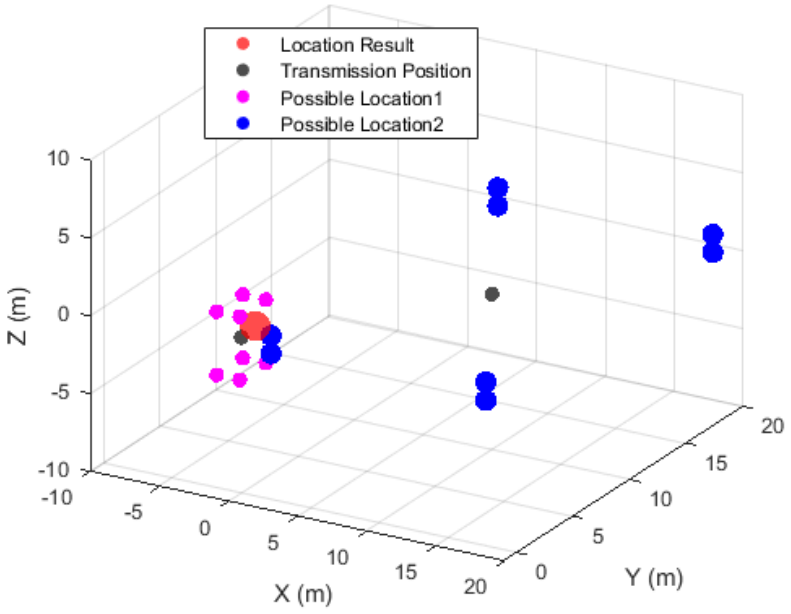


Figure 4. Possible results with theoretical voltage mixed with 5 dB SNR noise.

Since positioning errors occur in the presence of noise, it is necessary to process the voltage data to improve positioning accuracy. Under different signal-to-noise ratios, 100 groups of positioning data are generated. Positioning results are obtained using five methods: no filtering, Kalman filtering, traditional DBSCAN clustering, DBSCAN-MP clustering filtering, and DBSCAN combined with Kalman filtering. The visualization positioning results are shown in Figures 5–7. The dashed lines in these figures denote the error between actual positions and predicted values.

The average positioning error is defined as

$$e = \frac{1}{N}\sum_{i=1}^{N} \|\hat{\mathbf{p}}_i - \mathbf{p}_i\|_2 \tag{25}$$

where $\|,\|_2$ denotes the distance between two positions; $\mathbf{p}_i$ is the true position and $\hat{\mathbf{p}}_i$ is the estimated position, and $\mathbf{p}_i$ contains three-dimensional coordinates. Simulation results over 100 runs are summarized in Tables 2 and 3. At a high SNR of 20 dB, none of the clustering algorithms improve the positioning performance because the data points are close and indistinguishable. Kalman filtering slightly improves the positioning accuracy. At an SNR of 10 dB, traditional DBSCAN performs poorly, while the other methods achieve obvious improvement. At a low SNR of 5 dB, DBSCAN-MP and DBSCAN-MP+Kalman filtering achieve ideal performance, whereas the other methods are less effective. The above simulations verify that the proposed algorithm can effectively improve positioning performance under poor signal conditions when measurement errors are neglected. Figure 8 shows the average positioning error of different algorithms.

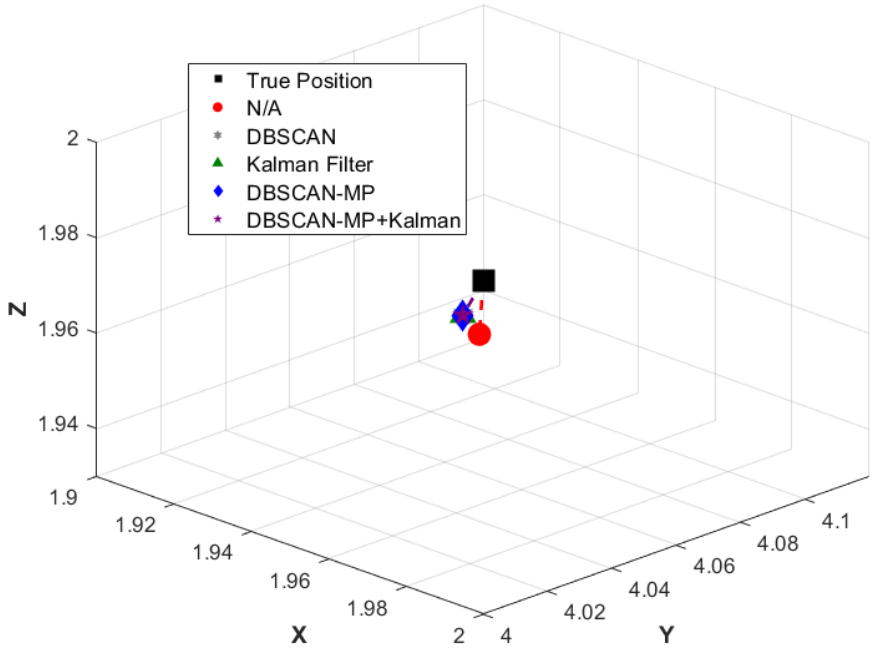


Figure 5. 3D localization results with 20 dB SNR noise.

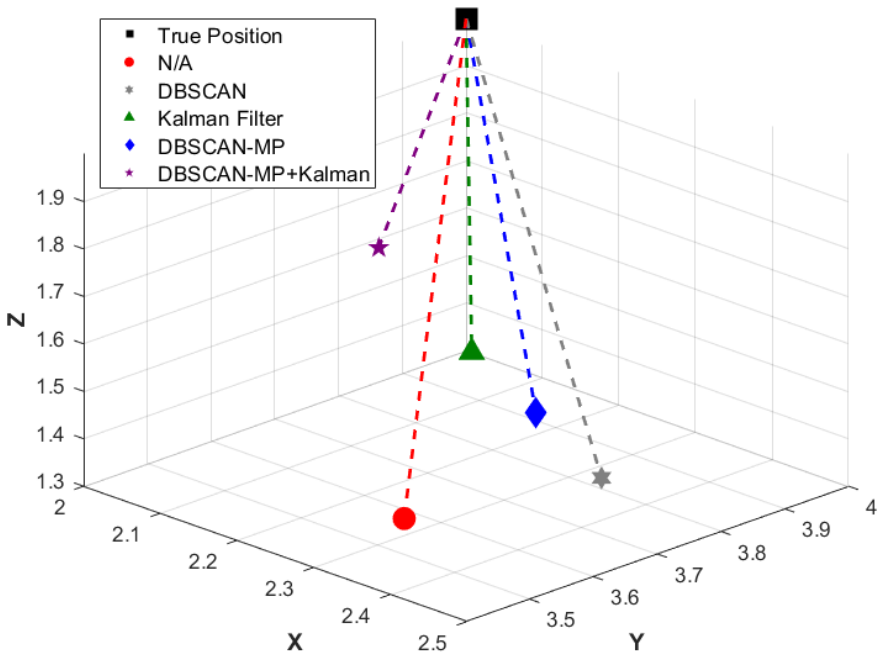


Figure 6. 3D localization results with 10 dB SNR noise.

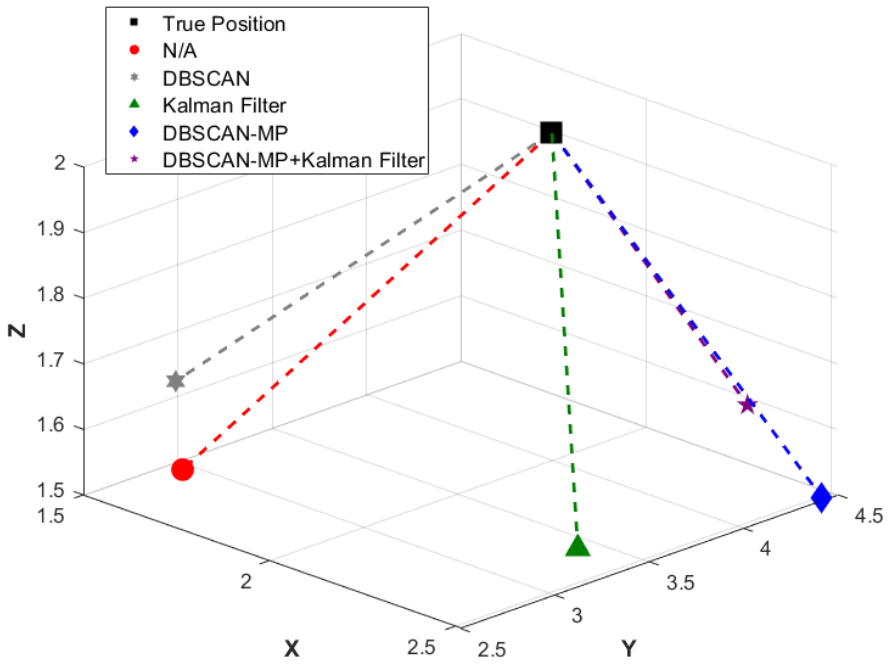


Figure 7. 3D localization results with 5 dB SNR noise.

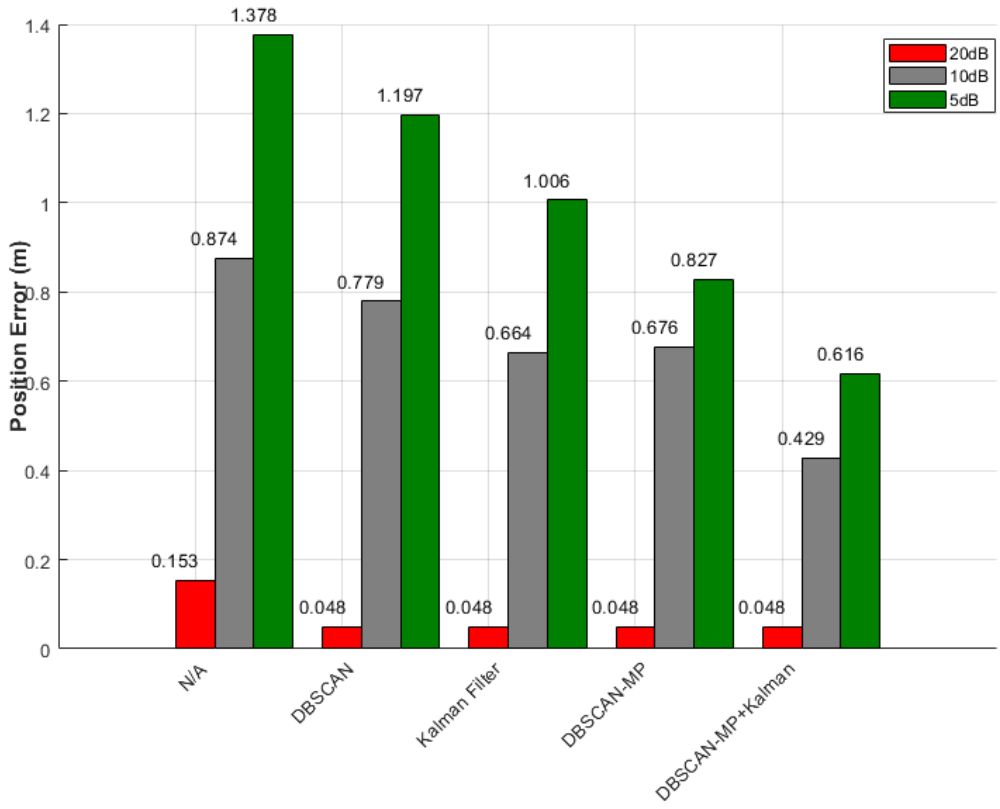


Figure 8. Average positioning error with different localization algorithms.

Table 2. Simulation positioning results (meters).

SNR	Raw	DBSCAN	Kalman	DBSCAN-MP	DBSCAN-MP+Kalman
20 dB	[1.91, 4.11, 1.94]	[1.97, 4.03, 1.98]	[1.97, 4.03, 1.98]	[1.97, 4.03, 1.98]	[1.97, 4.03, 1.98]
10 dB	[2.36, 3.47, 1.40]	[2.41, 3.72, 1.40]	[2.04, 3.96, 1.34]	[2.24, 3.82, 1.40]	[2.02, 3.84, 1.60]
5 dB	[1.64, 2.75, 1.54]	[1.51, 2.98, 1.63]	[2.46, 3.23, 1.54]	[2.52, 4.41, 1.50]	[2.36, 4.33, 1.62]

Table 3. Average positioning errors in simulation (meter).

SNR	Raw	DBSCAN	Kalman	DBSCAN-MP	DBSCAN-MP+Kalman
20 dB	0.1530	0.1530	0.0478	0.1530	0.0478
10 dB	0.8744	0.7791	0.6635	0.6758	0.4288
5 dB	1.3775	1.1970	1.0063	0.8268	0.6157

4.2. Indoor and Pool Experiments

The test site is located in a teaching building, as shown in Figure 9, two beacon devices B_1 and B_2 are placed at $[0, 0, 0]$ and $[8, 8, 0]$. The receiver R communicates with B_1 and B_2 in an 8 m $\times$ 8 m area. Communication data are encoded by Manchester code, ensuring equal high- and low-level durations on the coils. Positioning is performed by collecting voltage data on the receiver, with 100 rounds recorded at each point.

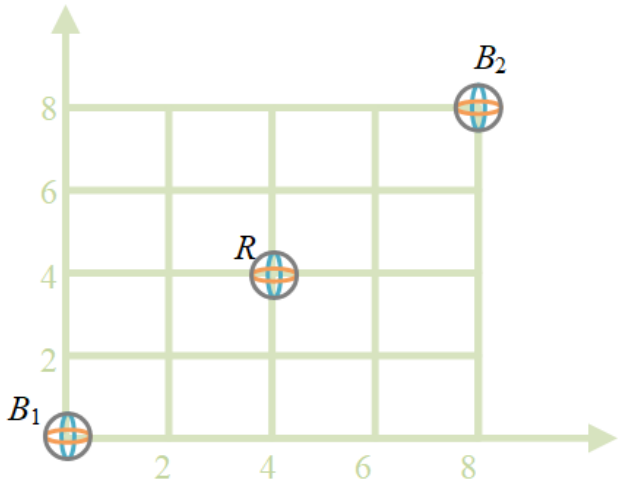


Figure 9. Indoor test scene.

Four processing schemes are compared: raw data, Kalman filtering, DBSCAN-MP clustering, and DBSCAN-MP plus Kalman filtering. The positioning results of 100 rounds are listed in Table 4.

Table 4. Experimental positioning results (unit: meters).

True Position	Raw	Kalman	DBSCAN-MP	DBSCAN-MP+Kalman
[2, 2, 0]	[3.1191, 0.3091, 0.0000]	[2.7296, 1.1229, 0.0000]	[2.5036, 1.3314, 0.0000]	[2.4624, 1.3102, 0.0000]
[2, 4, 0]	[1.0750, 3.9870, 0.0000]	[0.9638, 4.0507, 0.0000]	[1.5357, 3.7771, 0.0000]	[1.5206, 3.7906, 0.0000]
[2, 6, 0]	[3.2988, 4.4748, 0.0000]	[3.3047, 4.4707, 0.0000]	[2.7530, 5.6742, 0.0000]	[2.7430, 5.7571, 0.0000]
[4, 2, 0]	[2.2793, 2.9021, 0.0000]	[3.1101, 2.2763, 0.0000]	[3.4924, 2.0085, 0.0000]	[3.4761, 1.9966, 0.0000]
[4, 4, 0]	[4.3271, 1.5517, 0.0000]	[4.1678, 1.7392, 0.0000]	[3.3087, 3.3516, 0.0000]	[3.5952, 3.3374, 0.0000]
[4, 6, 0]	[2.6477, 4.7682, 0.0000]	[3.1347, 4.8479, 0.0000]	[3.4129, 5.3688, 0.0000]	[3.5314, 5.4901, 0.0000]
[6, 2, 0]	[4.1486, 3.5801, 0.0000]	[4.5937, 3.2132, 0.0000]	[5.0884, 2.1644, 0.0000]	[5.2380, 2.0849, 0.0000]
[6, 4, 0]	[4.2970, 4.6754, 0.0000]	[4.7747, 4.7963, 0.0000]	[5.3747, 4.3677, 0.0000]	[5.4047, 4.3277, 0.0000]
[6, 6, 0]	[3.7342, 5.3320, 0.0000]	[4.4687, 5.4633, 0.0000]	[5.2903, 5.5277, 0.0000]	[5.6077, 5.7406, 0.0000]
[2, 2, 2]	[1.7072, 2.8673, 1.7610]	[1.7728, 2.8676, 1.6905]	[2.3159, 2.4434, 1.6619]	[2.3301, 2.4253, 1.6630]
[3, 3, 2]	[4.0214, 1.7155, 1.2392]	[4.0667, 1.7891, 1.1524]	[3.5066, 2.6717, 1.4936]	[3.4984, 2.6593, 1.4845]

The average positioning error is derived as

$$e = \frac{1}{N} \sum_{i=1}^{N} \left\| \hat{\mathbf{p}}_i - \mathbf{p}_i \right\|_2 \tag{26}$$

where $\mathbf{p}_i$ is the true position and $\hat{\mathbf{p}}_i$ is the estimated position. The average errors are listed in Table 5 and Figure 10.

Table 5. Average positioning errors (unit: meters).

True Value	Raw	Kalman	DBSCAN-MP	DBSCAN-MP+Kalman
[2, 2, 0]	2.1450	1.1409	0.8376	0.8304
[2, 4, 0]	1.1978	1.0375	0.8283	0.5232
[2, 6, 0]	2.0112	2.0102	0.8204	0.7816
[4, 2, 0]	2.0054	0.9318	0.6711	0.5239
[4, 4, 0]	2.8431	2.2670	0.9487	0.7764
[4, 6, 0]	1.8919	1.4408	0.8620	0.6925
[6, 2, 0]	2.4592	1.8412	0.9506	0.7667
[6, 4, 0]	2.7861	1.8573	0.7253	0.6771
[6, 6, 0]	2.3657	1.6226	0.8524	0.4703
[2, 2, 2]	1.6032	0.9488	0.9914	0.6352
[3, 3, 2]	2.4954	1.8228	1.2090	0.7938

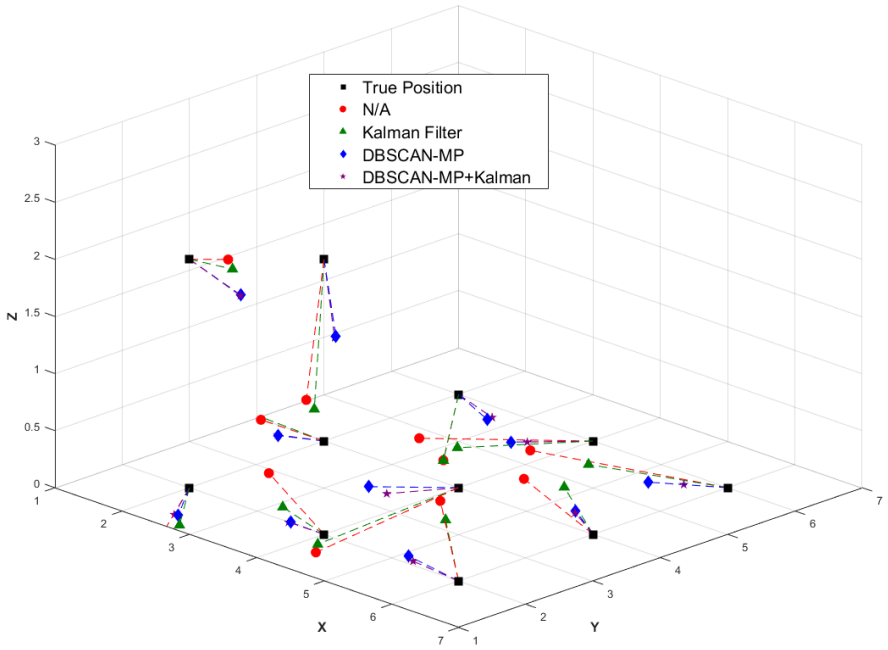


Figure 10. Each site's positioning results with different localization algorithms.

It can be observed that raw data yield large errors due to outliers. Kalman filtering alone reduces errors to the meter level. After DBSCAN-MP clustering, errors decrease significantly. Residual errors are caused by sensor precision, magnetic interference, coil alignment bias, and underwater path loss. With DBSCAN-MP plus Kalman filtering, the overall average error reaches 0.67 m and maximum error 0.83 m, achieving sub-meter accuracy.

The positioning errors of all positioning points (including 11 sites) in Figure 11 are averaged to obtain the mean errors of the positioning results for different algorithms. The mean error without any processing is extremely large, as the outliers significantly degrade the positioning accuracy. Direct application of the Kalman filter yields meter-level positioning error. After clustering with the proposed DBSCAN-MP algorithm, the mean error is substantially reduced. When combined with the Kalman filter, the DBSCAN-MP+Kalman filter method achieves sub-meter-level accuracy, with an average positioning error of 0.67 m and a maximum positioning error of 0.83 m. The average positioning error is defined as the mean positioning error calculated from multiple tested positioning points,

and the maximum positioning error is defined as the maximum positioning error of all measured positioning points.

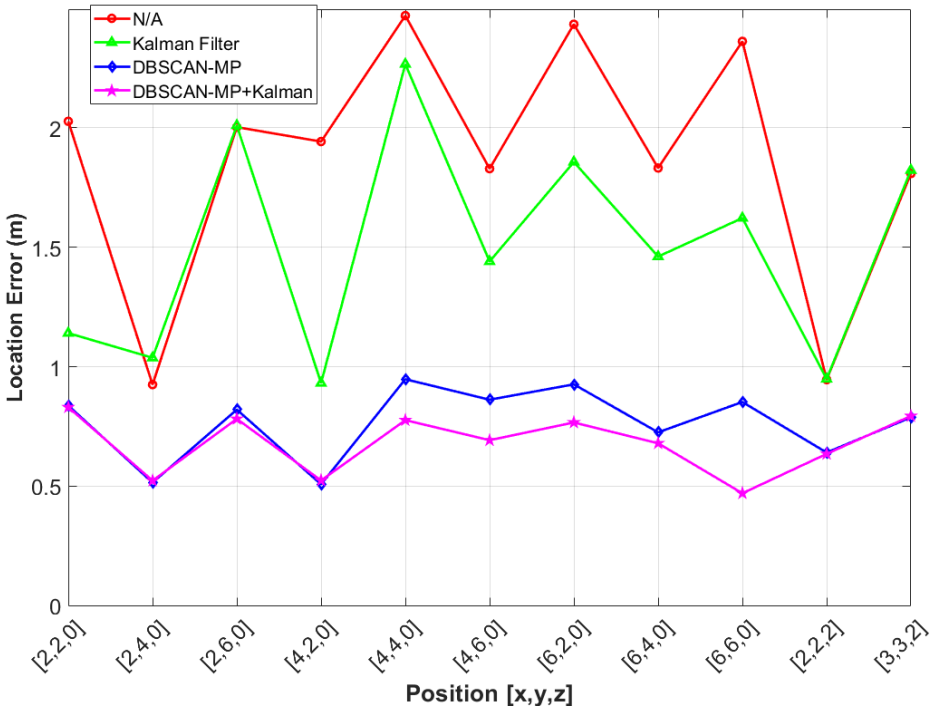


Figure 11. Each site's positioning error with different localization algorithms.

Figure 12 shows the average positioning error of different algorithms. It is obvious that the position errors derived from our algorithm are lower than those of these existing algorithms.

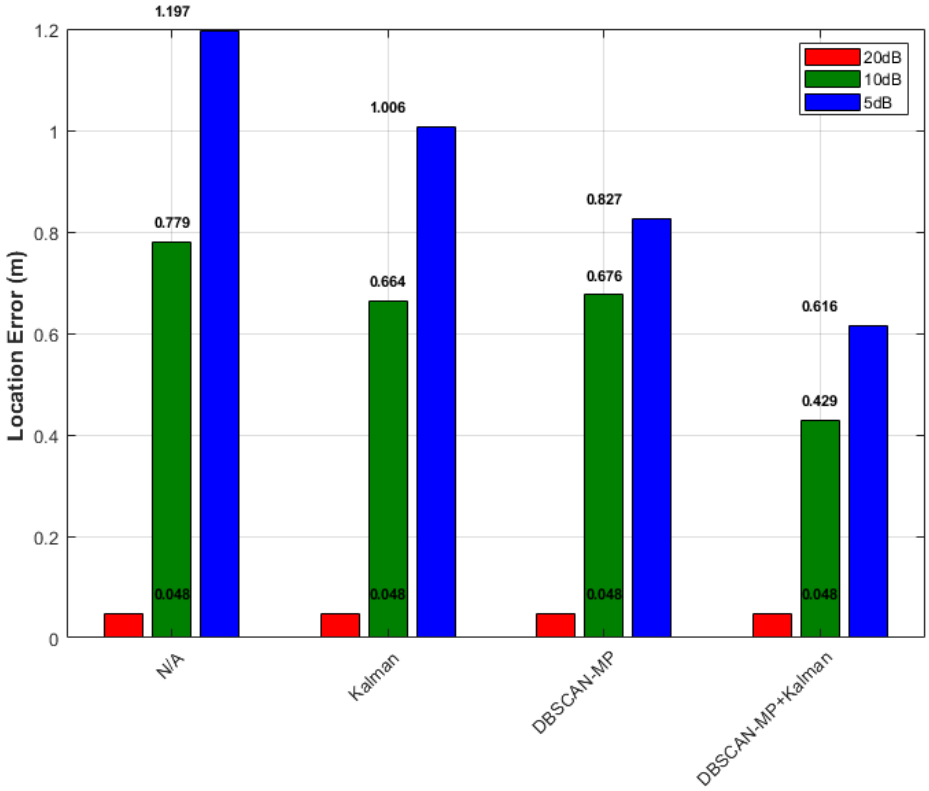


Figure 12. Average positioning error with different localization algorithms.

Table 6 compares the proposed method with state-of-the-art magnetic positioning systems. The average error is moderate, limited by ADC precision. However, the maximum error of 0.83 m is competitive, and the proposed method provides stable performance across multiple test points.

Table 6. Performance comparison of magnetic positioning methods.

Ref.	Size	Avg Error	Max Error
Pasku [8]	15 m × 12 m	0.3 m	0.9 m
Hehn [13]	7 m × 5 m × 3 m	∼1 m	—
Li [14]	8.4 m × 6.5 m	—	0.83 m
Yeh [15]	31 m × 10 m	0.76 m	—
Wang [16]	∼43 m × 43 m	1.02 m	3.85 m
Li [17]	5.4 m × 5.4 m	0.6–1.34 m	1.34 m
Proposed	8 m × 8 m	0.67 m	0.83 m

Moreover, the positioning test is conducted in an underwater environment, as shown in Figure 13. The positioning results achieve sub-meter-level accuracy, which meets the expected performance requirements.

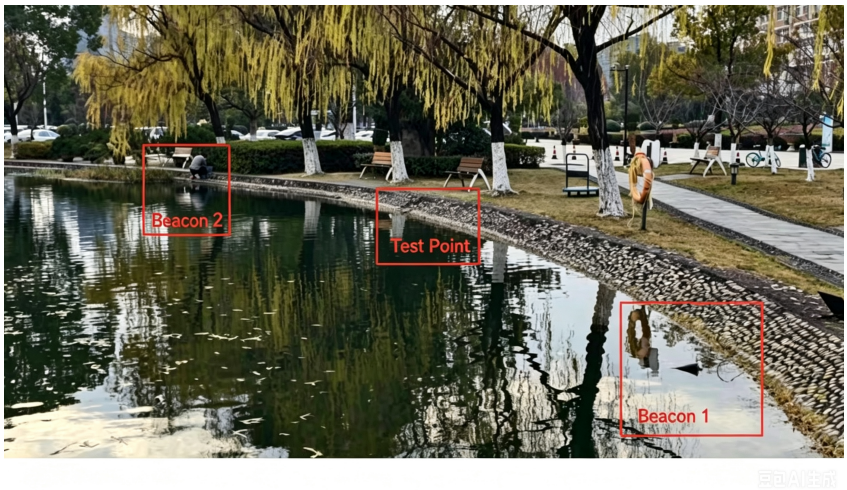


Figure 13. Underwater positioning test scenario.

5. Conclusions

This paper presents an underwater 3D localization method using dual 3D magnetic beacons and a DBSCAN-MP + Kalman filtering framework, where an improved density clustering algorithm, DBSCAN-MP, is proposed to remove erroneous positioning data. Simulation and experimental results demonstrate that the average positioning error of the proposed localization method is 0.67 m and the maximum positioning error is 0.83 m. The proposed method achieves stable sub-meter accuracy. Our future works will improve hardware precision and verify dynamic localization.

Author Contributions: Conceptualization, W.C. and N.Z.; methodology, N.Z.; validation, M.Z.; investigation, M.Z., N.A. and Z.Y.; resources, N.A.; writing—original draft preparation, W.C. and N.Z.; writing—review and editing, W.C.; visualization, M.Z.; supervision, M.Z.; project administration, M.Z.; funding acquisition, W.C, Z.Y. All authors have read and agreed to the published version of the manuscript.

Funding: This research has been partially supported by the Natural Science Foundation of Zhejiang Province (LMS26F010019), National Natural Science Foundation of China (No. 62271179), and Scientific research foundation of Zhejiang University of Water Resources and Electric Power (JBGS2025008).

Data Availability Statement: The data presented in this study are available on request from the corresponding author.

Conflicts of Interest: Author Zhou Yu was employed by Hangzhou Aohai Ocean Engineering Technology Co., Ltd. The remaining authors declare that the research was conducted in the absence of any commercial or financial relationships that could be construed as a potential conflict of interest.

References

1. Pan, D.; Lin, S.; Jin, Y.; Wang, J.; Jin, C.; Wang, Y.; Wang, L.; Li, L. Avoidance method of magnetic target positioning-inaccuracy-area. *IEEE Trans. Instrum. Meas.* **2023**, *73*, 6003409. [CrossRef]
2. Muzzammil, M.; Al-Kuwari, S.; Ahmed, N.; Qaraqe, M. Full-Duplex Magnetic Induction Communication: Opportunities and Challenges. *IEEE Wirel. Commun.* **2023**, *31*, 293–298. [CrossRef]
3. Abrudan, T.E.; Kypris, O.; Trigoni, N.; Markham, A. Impact of rocks and minerals on underground magneto-inductive communication and localization. *IEEE Access* **2016**, *4*, 3999–4010. [CrossRef]
4. Abrudan, T.E.; Xiao, Z.; Markham, A.; Trigoni, N. Underground incrementally deployed magneto-inductive 3-D positioning network. *IEEE Trans. Geosci. Remote Sens.* **2016**, *54*, 4376–4391.
5. Chavda, M.; Zeeshan, M.; O'Sullivan, C.; Holmes, A.S.; Malik, S. Magnetic-induction-based positioning system using dual multiplexing technique. *IEEE Sens. Lett.* **2023**, *7*, 5502404.
6. Wang, C. Research on Radiation-Resistant Underwater Robot Positioning System Based on 3D Electromagnetic Coils. Master's. Thesis, University of Electronic Science and Technology of China, Chengdu, China, 2023.
7. Huang, H.; Zheng, Y.R. Node localization in 3-D by magnetic-induction communications in wireless sensor networks. In *OCEANS 2017-Anchorage*; IEEE: Piscataway, NJ, USA, 2017; pp. 1–6.
8. Pasku, V.; De Angelis, A.; Moschitta, A.; Carbone, P.; Nilsson, J.O.; Dwivedi, S.; Händel, P. A magnetic ranging-aided dead-reckoning positioning system for pedestrian applications. *IEEE Trans. Instrum. Meas.* **2017**, *66*, 953–963. [CrossRef]
9. Hehn, M.; Sippel, E.; Carlowitz, C.; Vossiek, M. High-accuracy localization and calibration for 5-DoF indoor magnetic positioning systems. *IEEE Trans. Instrum. Meas.* **2018**, *68*, 4135–4145.
10. Blakely, R.J. *Potential Theory in Gravity and Magnetic Applications*; Cambridge University Press: Cambridge, UK, 2001.
11. Domingo, M.C. Magnetic induction for underwater wireless communication networks. *IEEE Trans. Antennas Propag.* **2012**, *60*, 2929–2939. [CrossRef]
12. Li, Q.; Li, X.; Wang, C.; Wang, Z.; Wen, F.; Zhao, Z. An inertial magneto-inductive positioning system based on GWO-PF algorithm. *IEEE Trans. Instrum. Meas.* **2022**, *71*, 9509510.
13. Yeh, S.C.; Hsu, W.H.; Lin, W.Y.; Wu, Y.F. Study on an indoor positioning system using Earth's magnetic field. *IEEE Trans. Instrum. Meas.* **2019**, *69*, 865–872. [CrossRef]
14. Wang, Z.; Yang, Z.; Wang, Z. An adaptive indoor positioning method using multisource information fusion combing Wi-Fi/MM/PDR. *IEEE Sens. J.* **2022**, 22, 6010–6018. [CrossRef]
15. Li, K.; Gong, Q.; Ren, Y.; Li, Y.; Han, Y.; Pang, C.; Kong, H. Magnetic field positioning technology for indoor sports objects. *IEEE Sens. J.* **2021**, 22, 219–228.
16. Muzzammil, M.; Ahmed, N.; Qiao, G.; Ullah, I.; Wan, L. Fundamentals and Advancements of Magnetic-Field Communication for Underwater Wireless Sensor Networks. *IEEE Trans. Antennas Propag.* **2020**, 68, 7555–7570. [CrossRef]
17. Qiao, G.; Zhao, C.; Zhou, F.; Ahmed, N. Distributed Localization Based on Signal Propagation Loss for Underwater Sensor Networks. *IEEE Access* **2019**, *7*, 112985–112995. [CrossRef]

Disclaimer/Publisher's Note: The statements, opinions and data contained in all publications are solely those of the individual author(s) and contributor(s) and not of MDPI and/or the editor(s). MDPI and/or the editor(s) disclaim responsibility for any injury to people or property resulting from any ideas, methods, instructions or products referred to in the content.